International Journal of Thermophysics, Vol. 27, No. 6, November 2006 (© 2006)
DOI: 10.1007/s10765-006-0086-6

Thermal Conductivity of Carbon Aerogels as a Function of Pyrolysis Temperature[1]

M. Wiener,[2,3] G. Reichenauer,[2,4] F. Hemberger,[4] and H.-P. Ebert[4]

Amorphous carbon samples with a total porosity of about 85% were synthesized via pyrolysis of sol–gel derived resin precursors. Since the pores in the samples investigated have dimensions of a few tens of nanometers only, the gaseous contribution to the thermal conductivity is largely suppressed at ambient pressure. Values for the total thermal conductivity as low as $0.054\,W{\cdot}m^{-1}{\cdot}K^{-1}$ at 300°C are detected. However, the pyrolysis temperature has a great impact on the contribution of the solid backbone to the total thermal conductivity. From the same precursor a series of samples was prepared via pyrolysis at temperatures ranging from 800 to 2500°C. The thermal conductivity of this series of carbons at 300°C under vacuum increases by a factor of about 8 if the pyrolysis temperature is shifted from 800 to 2500°C. To elucidate the reason for this strong increase, the infrared radiative properties, the electrical conductivity, the macroscopic density, the microcrystallite size, the sound velocity, and the inner surface of the samples were determined. Evaluation of the experimental data yields only a negligible contribution from radiative heat transfer and electronic transport to the total thermal conductivity. The main part of the increasing thermal conductivity therefore has to be attributed to an increasing phonon mean free path in the carbons prepared at higher pyrolysis temperatures. However, the phonon mean free path does not match directly the in-plane microcrystallite size of the amorphous carbon. Rather, the in-plane microcrystallite size represents an upper limit for the phonon mean free path. Hence, the limiting factor for the heat transport via phonons has to be defects within the carbon microcrystallites which are partially cured at higher temperatures.

KEY WORDS: aerogels; amorphous carbon; mean free path; microcrystallites; pyrolysis temperature; thermal conductivity.

[1] Paper presented at the Seventeenth European Conference on Thermophysical Properties, September 5–8, 2005, Bratislava, Slovak Republic.

[2] Physics Department, Würzburg University, Am Hubland, 97074 Würzburg, Germany.
[3] To whom correspondence should be addressed. E-mail: matthias.wiener@zae.uni-wuerzburg.de
[4] Bavarian Center for Applied Energy Research, Am Hubland, 97074 Würzburg, Germany.

1. INTRODUCTION

The amorphous carbons investigated in this study were derived via pyrolysis of highly porous resorcinol formaldehyde resins according to the sol–gel route first published by Pekala and Kong [1]. This type of material is also called carbon aerogels or xerogels. Besides the application of carbon aerogels as electrodes in supercapacitors [2, 3] or gas diffusion layers in fuel cells [4, 5], they are promising materials for high temperature thermal insulation. The morphology of a typical carbon aerogel is shown in Fig. 1. The picture shows a network of interconnected spherical primary particles that defines an interconnected pore phase. By varying the synthesis parameters, i.e., by varying the composition of the starting solution and the process temperature of the sol–gel process, it is possible to tailor the particle and pore sizes in the range from a few nanometers up to some microns; applying ambient pressure drying of the gelled and cured resins, porosities up to 85% can be achieved. This is the key for thermally stable materials with exceptionally small thermal conductivities. However, the thermal conductivity of this type of amorphous carbon depends significantly on the pyrolysis temperature applied. In the past, other authors have studied the effects of high temperature treatment on the properties of hard carbons. Hanzawa et al. [6] and Soukup et al. [7] have investigated in detail the changes of microcrystallite properties in carbon aerogels and glassy carbon, respectively. Lu et al. [8] and Nilsson et al. [9] analyzed

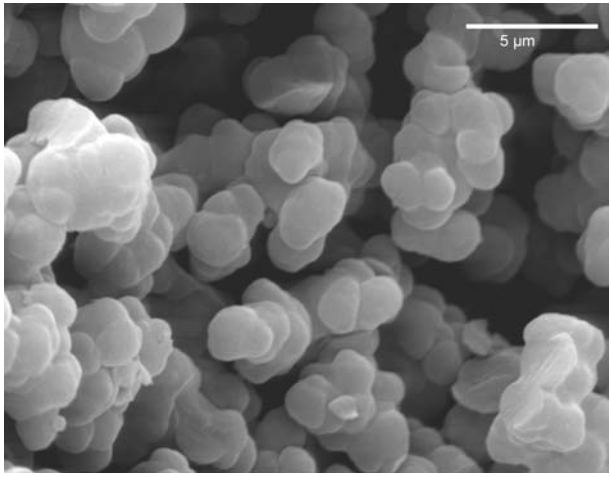

Fig. 1. SEM micrograph showing the typical morphology of a monolithic carbon aerogel with particle sizes around 1 µm and pore sizes in the 5 µm range.

the thermal conductivity of carbon aerogels as a function of temperature, and sample density and electrical conductivity, respectively. Bock et al. [10] investigated the thermal conductivity of carbon aerogels as a function of sample density and temperature as well as the in-plane microcrystallite size and phonon mean free path as a function of the sample density.

In this work we systematically analyze the changes of material properties, like the electrical conductivity, the sample density, the microcrystallite size, the sound velocity, and the inner surface as a function of the pyrolysis temperature and their impact on the total thermal conductivity.

2. EXPERIMENTAL

2.1. Sample Preparation

The series of amorphous carbon investigated in this work was derived via pyrolysis of the same organic precursor at different temperatures. The synthesis of carbon aerogels is described in detail elsewhere [11]. Briefly, the precursors were synthesized by adding sodium carbonate as a base catalyst to an aqueous solution of resorcinol and formaldehyde. The molar ratio of formaldehyde to resorcinol is 2:1, and the mass ratio of resorcinol and formaldehyde in the solution was chosen to yield a final density of about $300\,\mathrm{kg \cdot m^{-3}}$. First, the solution was filled in a vessel and sealed airtight; then it was exposed to 85°C for 24 h for gelling and curing. Afterwards, the pore liquid within the wet gel (essentially water) was replaced by ethanol (a liquid with lower surface tension) and the gel was dried at ambient conditions. The resulting organic aerogel was then cut into eight small cylinders of the same size (diameter = 21 mm; height = 6 mm). Each piece was finally pyrolized in an inert atmosphere at 800°C for the lowest and 2500°C for the highest final temperature, respectively (see Table I). A temperature ramp of $5^\circ\mathrm{C \cdot min^{-1}}$ was used; no dwell time was applied at the target temperature.

2.2. Sample Characterization

2.2.1. Density

The density of each sample was calculated from its dimensions and mass measured after heat treatment.

2.2.2. Electrical Conductivity

The electrical conductivity was measured with a four-wire setup in order to avoid contact resistance effects [3]. The current and voltage were measured with a HP 3457A multimeter. The voltage was tapped by two

Table I. Summary of Experimental Data for the Carbon Samples Pyrolyzed at Temperatures between 800 and 2500°C

Pyrolysis temperature (°C)	Density ($kg \cdot m^{-3}$)	Electrical conductivity ($S \cdot cm^{-1}$)	Micro-crystallite size L_a (Å)	Ultrasonic velocity ($m \cdot s^{-1}$)	S_{BET} ($m^2 \cdot g^{-1}$)	S_{ext} ($m^2 \cdot g^1$)	S_μ ($m^2 \cdot g^{-1}$)	V_μ ($cm^3 \cdot g^{-1}$)	Thermal Diffusivity a ($mm^2 \cdot s^{-1}$)
800	320	–	28	601	532	102	430	0.22	0.126
1000	323	2.84	32	695	571	97	473	0.24	0.206
1250	323	6.54	38	746	386	99	287	0.15	0.305
1500	307	7.2	44	716	267	98	169	0.09	0.415
1750	301	8.3	45	757	159	107	51	0.03	0.550
2000	303	8.72	43	717	133	110	23	0.01	0.725
2250	314	9.66	48	735	120	106	14	0.01	0.925
2500	315	9.19	47	732	123	101	22	0.01	0.990

sharp stainless steel pins mounted onto a movable measuring head. For each sample three measurements were performed at different locations of the sample and the values were averaged to derive a mean value for the electrical conductivity.

2.2.3. *Microcrystallite size*

For the quantification of disordered graphitic structures and, in particular, for the characterization of microcrystallite sizes in carbon materials, Raman spectroscopy is a convenient method. The spectra were measured using the 488-nm line of an argon ion laser, and the power of excitation was adjusted to about 70 μW in order to prevent the sample surface from degradation or heating during measurement. In the experiment a range in wave numbers from 700 to 2000 cm^{-1} was covered. A typical Raman plot is shown in Fig. 2. There are two dominant bands in the spectrum, one at about 1360 cm^{-1} associated with edge planes of microcrystallites and the Raman-active $E_{2g}^{(2)}$ mode at 1582 cm^{-1} [12]. According to the empirical formula of Knight and White [13], it is possible to extract the in-plane microcrystallite size L_a via the following relationship:

$$L_a(\text{Å}) = 44(I_{1582}/I_{1360}), \tag{1}$$

where I_{1360} and I_{1582} are the integrated intensities of the respective peaks. To determine the integrated intensities the two bands were fitted to a

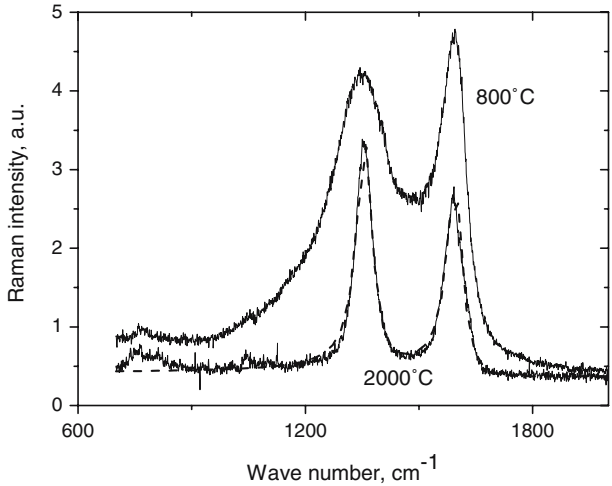

Fig. 2. Raman spectra of carbon aerogels pyrolyzed at 800 and 2000°C; dashed line is a fit of Eq. (2) to the experimental data of the sample pyrolyzed at 2000°C.

Breit–Wigner–Fano lineshape [14],

$$I(\upsilon) = \frac{I_0[1 + 2(\upsilon - \upsilon_0)/q\Gamma]^2}{1 + [2(\upsilon - \upsilon_0)/\Gamma]^2}, \tag{2}$$

where $I(\upsilon)$ is the intensity, υ_0 is the wave number at the peak, I_0 is the intensity at the peak position, Γ is the peak width at half-height, and $1/q$ is a parameter accounting for the interactions between the discrete $E_{2g}^{(2)}$ mode and a Raman-active continuum ($1/q = 0$ for Lorentzian line shape) [14].

2.2.4. Ultrasonic Velocity

The propagation of an ultrasonic signal across the sample was measured by a setup consisting of a piezo-transmitter operating at 0.5 MHz and a piezo receiver. The sample was clamped between the transmitter and the receiver, and the time delay was monitored by a HP 54601A oscilloscope. The sound velocity then was calculated from the sample dimension divided by time delay.

2.2.5. Extinction Coefficient

To determine the infrared-optical extinction coefficient, the spectral–hemispherical transmittance T_{dh} and reflectance R_{dh} of the samples were measured by the integrating sphere method for wavelengths between 2 and 18 μm. From T_{dh} and R_{dh} the scaled mass specific scattering coefficient s^* and the mass specific absorption coefficient a can be derived via the three-flux method [15]. Finally, the scaled specific extinction coefficient e^* can be calculated according to

$$e^* = a + s^*. \tag{3}$$

2.2.6. Surface Area and Pore Volume

The surface area and pore volume of each sample were determined via N_2-sorption measurements at 77 K using a Micromeritics ASAP 2000 apparatus. Prior to adsorption the samples were degassed at 110°C under vacuum for at least 12 h. Figure 3 depicts a typical nitrogen adsorption/desorption isotherm of one of the carbons investigated.

By applying different evaluation methods, it is possible to distinguish between the "inner" surface area of the sample due to micropores (< 2 nm) and the "external" surface area due to meso- or macropores (> 2 nm). From the isotherm the total specific surface area S_{BET} of the sample was calculated by applying the Brunauer–Emmet–Teller method [16] in the relative pressure range between 0.1 and 0.26. In addition, the external surface area S_{ext} (due to meso- or macropores) was determined from the slope of

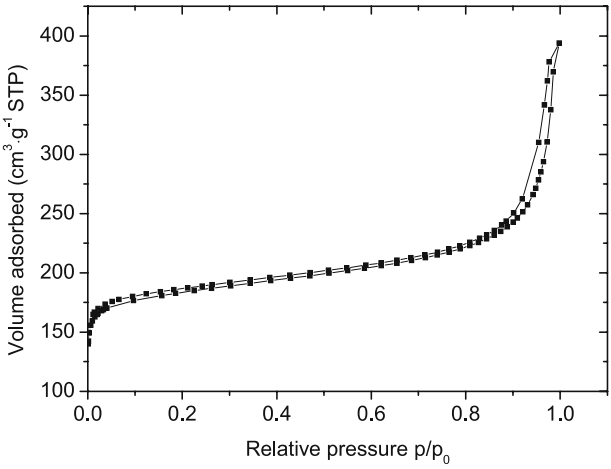

Fig. 3. Nitrogen sorption isotherm of the carbon sample pyrolyzed at 1000°C.

the linear region of the t-plot. The micropore surface area S_μ was then calculated using $S_\mu = S_{BET} - S_{ext}$. The micropore volume V_μ was derived from the intercept of the linear slope of the t-plot with the ordinate.

2.2.7. Thermal Conductivity

The thermal properties of the series of samples were determined by the laser flash method. The measurements were performed under vacuum at 300°C in order to exclude contributions due to gaseous conductivity and adsorbed molecules at the inner surface of the porous samples. The front side of the sample was thermally excited by a laser flash pulse (NdYaG-laser, 1064 nm). The back-side temperature was monitored by a MCT infrared detector as a function of time. The assembly of the laser flash apparatus used is described in detail elsewhere [17]. From the time dependence of the signal the thermal diffusivity a is determined [18]. With a known specific heat capacity c_p, the thermal conductivity λ of the material can be calculated from

$$\lambda(T, T_P) = a(T, T_P)\rho(T_P)c_p(T). \tag{4}$$

Here T is the temperature at which the thermal measurement is performed and T_P is the temperature applied to the samples upon pyrolysis. The values for the specific heat c_p below 200°C were determined under argon by temperature modulated differential scanning calorimetry (MDSC) (Fig. 4); above 200°C, literature values were used [19]. It can be seen that the two curves coincide in the range around 200°C.

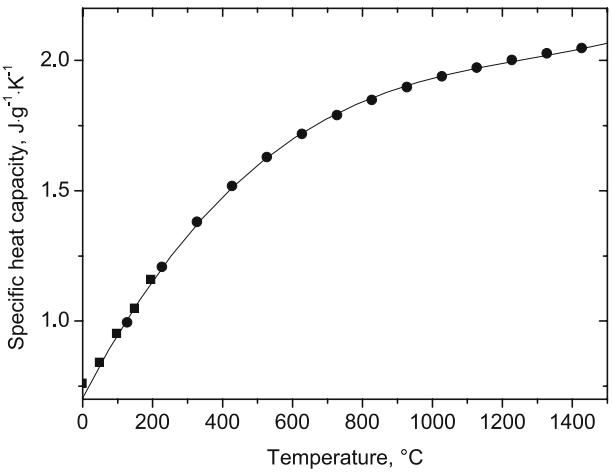

Fig. 4. Specific heat capacity c_p as a function of temperature: (■) experimental values determined by dynamic difference calorimetry; (•) data taken from literature [19]; and line represents a polynomial fit to the data.

3. THEORETICAL BACKGROUND

Generally, the heat transport through a porous solid consists of a radiative, a gaseous, and a solid contribution. The radiative thermal conductivity λ_{rad} can be calculated according to

$$\lambda_{\text{rad}} = \frac{16\sigma n^2}{3\rho e} T^3. \tag{5}$$

Hereby σ is the Stefan–Boltzmann constant, $n \approx 2$ is the refractive index for carbon, T is the temperature, ρ is the sample density, and e is the mass specific extinction coefficient (see Eq. (3)).

The solid thermal conductivity can be expressed in a first-order approximation by the sum of the electronic contribution λ_{el} and the phononic contribution λ_{ph}. The electronic thermal conductivity for metals and semimetals can be described by the Wiedemann–Franz law [20],

$$\lambda_{\text{el}} = \sigma_{\text{el}} L T, \tag{6}$$

where σ_{el} is the electrical conductivity and L is the Lorentz number.

The phononic contribution to the thermal conductivity in the solid phase is given by [21]

$$\lambda_{\text{ph}} = \frac{1}{3}\rho c_v v_{\text{ph}} l, \tag{7}$$

where $c_v \approx c_p$, v_{ph} is an average phonon velocity, and l is the mean free path of the phonons.

4. RESULTS

All experimentally determined data are summarized in Table I.

4.1. Density

The density of the series of carbons was determined as a function of pyrolysis temperature (Fig. 5). The experimental results for the different samples vary between 301 and 323 $kg \cdot m^{-3}$. However, within the given uncertainty of 4% the density can be assumed to be independent of the pyrolysis temperature and is therefore set to $(312 \pm 11)\,kg \cdot m^{-3}$ in the further course of this paper.

4.2. Electrical Conductivity

The electrical conductivities of the carbons as a function of the pyrolysis temperature are shown in Fig. 6. For samples pyrolyzed up to 1250°C the electrical conductivity rises significantly from 3 $S \cdot cm^{-1}$ at 1000°C to about 6.5 $S \cdot cm^{-1}$; beyond 1250°C, the electrical conductivity increases moderately to about 9 $S \cdot cm^{-1}$. These values correspond to the electrical

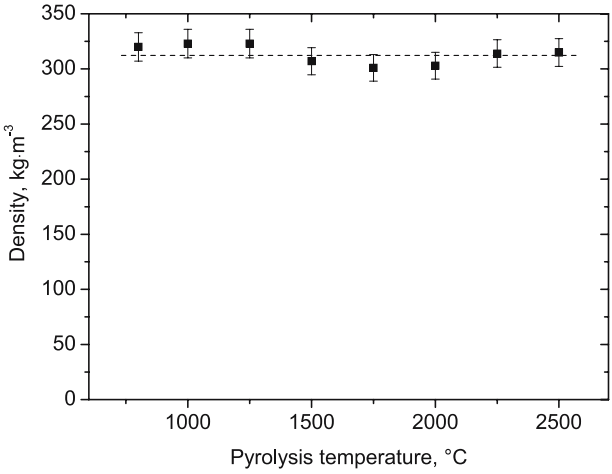

Fig. 5. Sample densities as a function of temperature treatment; dashed line corresponds to the mean value of all samples.

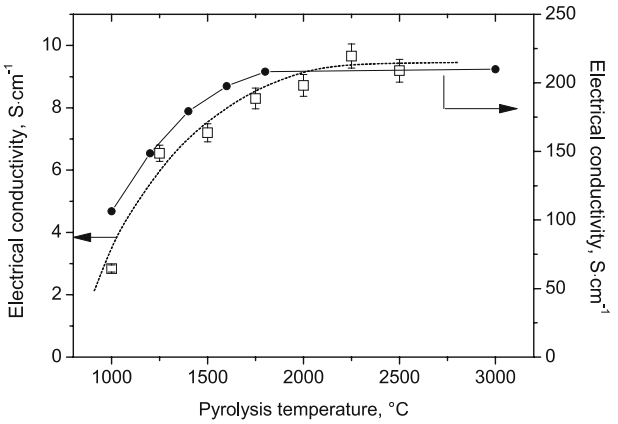

Fig. 6. Electrical conductivity of carbon aerogels as a function of pyrolysis temperature (□); dashed line is a guide to the eye. For comparison, values determined by Soukup et al. [7] for glassy carbon are plotted (•). Due to the higher density of the glassy carbon (a factor of about 5 compared to the aerogel), the electrical conductivity is significantly increased (note the corresponding second axis on the right).

conductivities reported by Lu et al. [8] for supercritically dried carbon aerogels with comparable densities. Soukup et al. [7] also observed a tendency to saturation in electrical conductivity for heat treatment temperatures above 1800°C when investigating glassy carbons, the dense version of carbon aerogels (Fig. 6).

4.3. Microcrystallite Size

Primary particles building the skeleton of hard carbons consist of a disordered system of graphene microcrystallites (house-of-cards model) [14]. The in-plane microcrystallite sizes L_a as determined via Eq. (1) from Raman data are given in Fig. 7. The average in-plane microcrystallite dimension L_a expands from 28 Å for a carbon sample pyrolyzed at 800°C to 47 Å for a sample pyrolyzed at 2500°C.

4.4. Ultrasonic Velocity

Morphological or structural changes caused by the temperature treatment affect the elastic properties and hence the sound velocity. In Fig. 8 the sound velocities of the samples pyrolyzed at temperatures between 800 and 2500°C are shown.

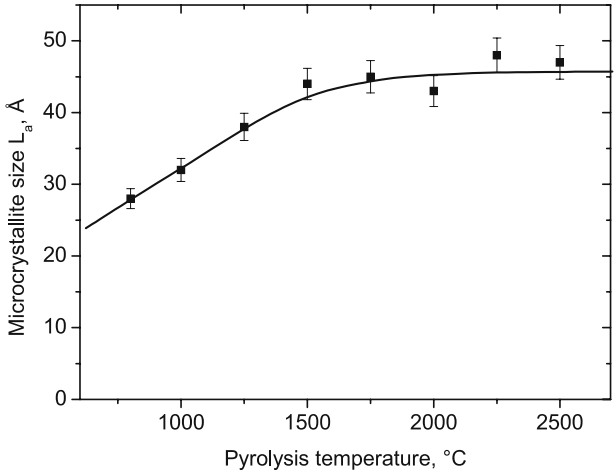

Fig. 7. In-plane microcrystallite size L_a of amorphous carbon samples as a function of pyrolysis temperature calculated from Raman data; full line is a guide to the eye.

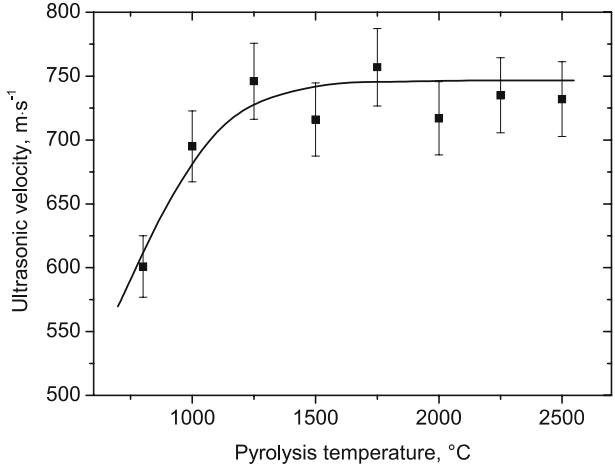

Fig. 8. Ultrasonic velocity as a function of treatment temperature; note that the zero is strongly suppressed. Full line is a guide to the eye.

The sound propagation velocity of the sample pyrolyzed at 800°C is about 600 $m \cdot s^{-1}$. For the sample treated at 1000°C the sound velocity rises to 700 $m \cdot s^{-1}$ and approaches about 720 $m \cdot s^{-1}$ for treatment temperatures of 1250°C and above.

4.5. IR-optical Extinction Coefficient

The measurements were performed with a Fourier transform infrared spectrometer combined with an external integrating sphere. The results for the scaled spectral scattering coefficient s^* and absorption coefficient a are shown in Fig. 9a for the two samples pyrolyzed at 800 and 2500°C. Using a suitable averaging procedure ("Rosseland" average), the mass specific extinction coefficient can be derived (Fig. 9b).

4.6. Surface Area and Pore Size

When increasing the pyrolysis temperature from 800 to 1000°C, nitrogen sorption yields an increase in total surface area S_{BET} from about 530 to 570 $m^2 \cdot g^{-1}$. Higher pyrolysis temperatures result in a decrease in S_{BET} down to about 150 $m^2 \cdot g^{-1}$. The micropore surface area S_μ shows the same trend indicating that the BET surface area is dominated by adsorption in micropores. In contrast, the external surface S_{ext} is almost unaffected by the treatment in the temperature range from 800 to 2500°C (see Fig. 10).

4.7. Thermal Conductivity

Figure 11 depicts the values of thermal conductivity at 300°C calculated via Eq. (4) from the laser flash results. The thermal conductivity for the sample pyrolyzed at 800°C is 0.05 $W \cdot m^{-1} \cdot K^{-1}$ at 300°C; the thermal conductivity increases continuously with the treatment temperature to 0.42 $W \cdot m^{-1} \cdot K^{-1}$ for the sample pyrolyzed at 2500°C. Figure 12 shows the thermal conductivity λ of a carbon sample pyrolyzed at 2000°C as a function of temperature. The experimental data were fitted with a linear superposition of phonon, electron, and radiative heat transfer ($\lambda_{total} = \lambda_{ph} + \lambda_{rad} + \lambda_{el} = \alpha C_P(T) + \beta T^3 + \gamma T$); the temperature dependence of the respective components is given by Eqs. (5) through (7). Figure 12 clearly exhibits that the thermal transport below 1000°C is dominated by the thermal conductivity of the solid phase. The electronic contribution is found to be negligible in the investigated range.

The fit parameters α and β are found to be 0.19 $g \cdot m^{-1} \cdot s^{-1}$ and 1.8×10^{-11} $W \cdot m^{-1} \cdot K^{-4}$, respectively. Using Eq. (7), α yields a mean free path of 25 Å. The extinction coefficient determined from parameter β via Eq. (5) is 230 $m^2 \cdot kg^{-1}$; this value is about a factor of 1.6 higher than the one determined via IR-spectroscopy (Fig. 9); this relatively large discrepancy, however, does not indicate a systematic deviation since the experimental temperature range (Fig. 12) is just too small to allow for a high enough accuracy in the extraction of the radiative contribution.

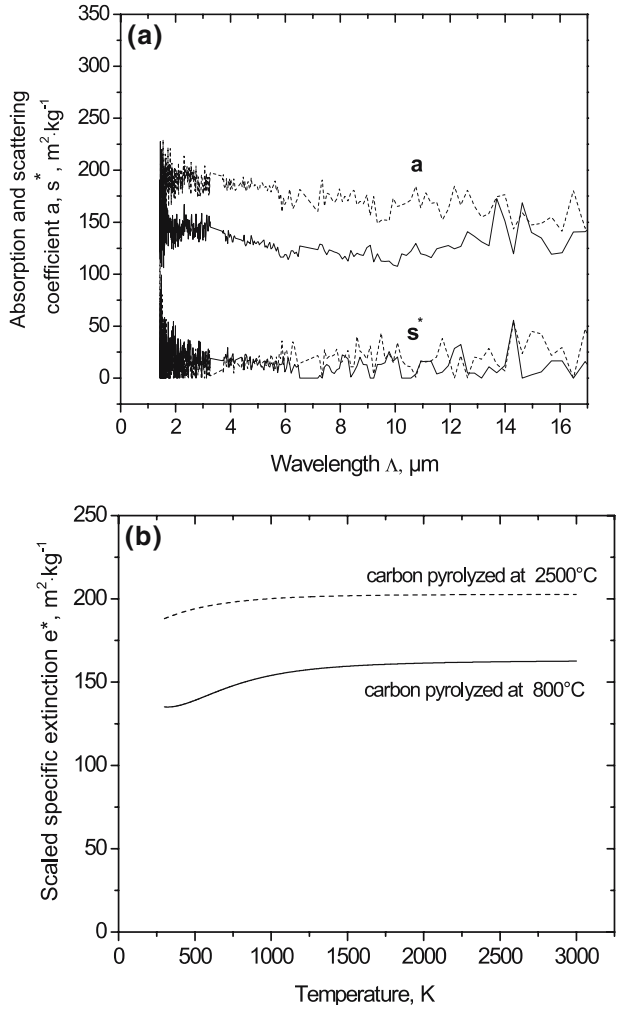

Fig. 9. (a) Scaled specific scattering coefficient s^* and specific absorption coefficient a vs. wavelength Λ for samples pyrolyzed at 800°C (——) and 2500°C (- - - - -), respectively and (b) scaled mass specific extinction coefficient for the two samples; data were derived via Rosseland averaging of the spectral data.

5. DISCUSSION

The heat transport through a porous solid consists of radiative, gaseous, and solid contributions. A change of thermal conductivity with pyrolysis temperature (Fig. 11) in the series of investigated samples caused

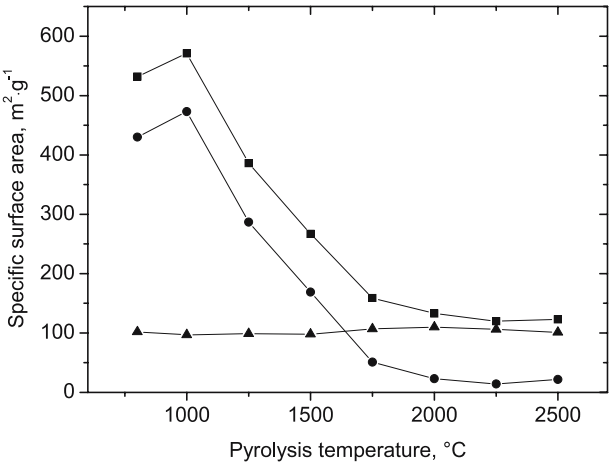

Fig. 10. Specific surface area as a function of pyrolysis temperature as derived from nitrogen sorption measurements: S_{BET}(■), S_{μ}(●), S_{ext}(▲).

by a change of the gaseous contribution can be excluded because the measurements were performed under vacuum.

The values calculated for the radiative contribution to the thermal conductivity at 300°C are found to be between $0.005\,W \cdot m^{-1} \cdot K^{-1}$ ($e \approx 140\,m^2 \cdot kg^{-1}$; see Fig. 9) for the sample pyrolyzed at 800°C and $0.004\,W \cdot m^{-1} \cdot K^{-1}$ ($e \approx 190\,m^2 \cdot kg^{-1}$; see Fig. 9) for the sample pyrolyzed at 2500°C. Both values are small compared to the total thermal conductivity (Fig. 11). This is also confirmed by the thermal conductivity measured as a function of temperature for the aerogel pyrolyzed at 2000°C (Fig. 12): The onset for the T^3-increase characteristic for radiative heat transfer (which is expected for a temperature independent extinction) first shows up above 1250°C. Therefore, the contribution of radiation cannot be responsible for the increase of the thermal conductivity at 300°C.

The change in thermal conductivity therefore has to be due to changes in the solid phase. However, modifications of the morphology of the porous carbon, like sintering processes affecting the meso- or macroporosity, obviously do not take place since otherwise the external surface of the samples investigated would not be constant (see Fig. 10). Similarly, the change in IR-extinction (Fig. 9) is mainly due to absorption while the scattering component that reflects the morphological characteristics of the samples is essentially unaffected by the pyrolysis temperature. In contrast, a modification of the solid on a length scale of 2 nm or less is obvious

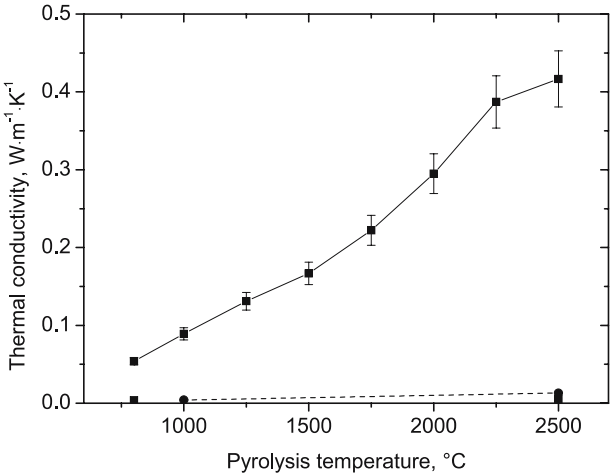

Fig. 11. Full line shows the thermal conductivity of carbon aerogels measured at 300°C under vacuum and pyrolyzed at temperatures between 800 and 2500°C. Data were calculated from thermal diffusivities derived via laser flash measurements. Dashed line corresponds to the electrical contribution to the thermal conductivity calculated via Eq. (6). Radiative contribution determined via Eq. (5) is too small to be visible in this representation.

by the variation of the micropore surface area S_μ determined by nitrogen sorption measurements (see Fig. 10) and the changes of the microcrystallite size (Fig. 7).

Generally, the solid thermal conductivity can contain both electronic and phononic contributions. According to [8] the Wiedemann–Franz law (Eq. (6)) should be applicable to the type of carbon samples investigated here. The values of the electrical contribution to the thermal conductivity calculated by Eq. (6) yield values between $0.004\,W{\cdot}m^{-1}{\cdot}K^{-1}$ for the sample heat treated at 1000°C and $0.013\,W{\cdot}m^{-1}{\cdot}K^{-1}$ for the sample heat treated at 2500°C. The value for 1000°C corresponds to that one found by Lu et al. [8] for a sample with similar density pyrolyzed at 1050°C. Although there is an obvious increase of the electrical contribution to the thermal conductivity caused by heat treatment, this contribution represents only a small effect compared to the experimental values for the thermal conductivity (Figs. 11 and 12).

The phononic thermal conductivity can be described by the phonon diffusion model (Eq. (7)). Assuming that the experimentally determined sound velocity v corresponds to the propagation velocity of the acoustic phonons v_{ph} within a solid, the phonon mean fee path l can be calculated from Eq. (4) according to

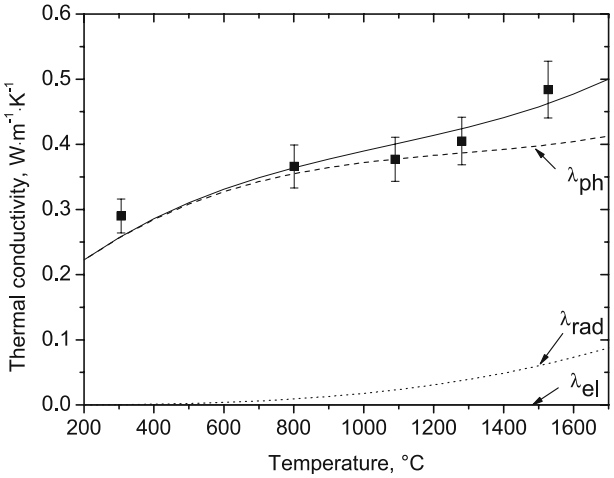

Fig. 12. Thermal conductivity as a function of temperature for the carbon sample pyrolyzed at 2000°C: full line is a fit of $\lambda_{total} = \lambda_{ph} + \lambda_{rad} + \lambda_{el}$ to the experimental data (see also Eqs. (5) through (7)); dashed line represents the solid conductivity; and dotted line indicates the contribution due to radiative heat transfer. Electronic contribution is too small to be visible in this representation.

$$l = \frac{3a}{v}. \tag{8}$$

Using Eq. (8) values for the mean free path l between 6 and 41 Å are obtained when the pyrolysis temperature is increasing from 800 to 2500°C (Fig. 13). These values correspond approximately to the data mentioned in [10]. However, in contrast to [10] the mean free paths l calculated in this work are without exception smaller than the microcrystallite size L_a determined from Raman measurements (Fig. 13). This implies that the mean free path of phonons in the samples under investigation is governed by defects smaller than the microcrystallite size. A similar effect has also been observed for the electrical conductivity in glassy carbons as a function of the pyrolysis temperature [7]. Small angle X-ray scattering investigation of carbon aerogels pyrolyzed at temperatures up to 2100°C reveal features that double in size from about 5 to 10 Å when the pyrolysis temperature increases from 1500 to 2100°C [22]. However, it is not clear whether the observed effect is due to a growth of micropores that are not accessible to nitrogen (see Fig. 10 and Table I) or a growth of the domains in the solid phase since the scattering only reflects a combined mean value of the extension of both phases.

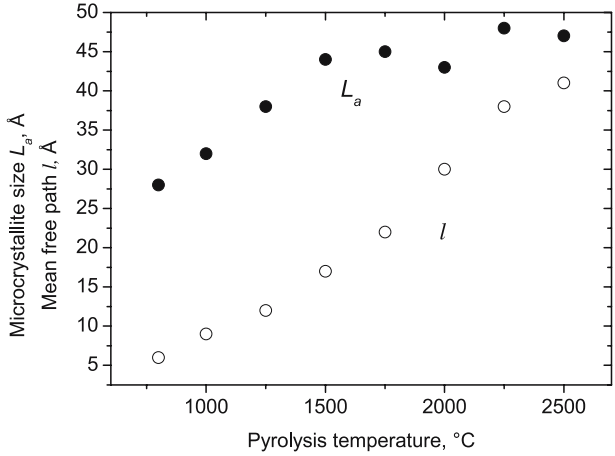

Fig. 13. Microcrystallite size L_a and mean free path l calculated via Eq. (8) as a function of pyrolysis temperature.

Comparing all physical properties determined as a function of pyrolysis temperature (Fig. 5 through 10) reveals that none of them shows a significant change above 1500°C, in contrast to the effect observed for the thermal conductivity (Fig. 11). Only the features detected by small angle scattering show a comparable change in the temperature range above 1500°C. This is a strong hint that these are the structural entities that are responsible for the huge increase of the solid thermal conductivity with pyrolysis temperature. Future investigations have to clarify this point.

6. SUMMARY

The thermal conductivity of amorphous carbon strongly depends on the maximal treatment/pyrolysis temperature. In a pyrolysis temperature range between 800 and 2500°C, the thermal conductivity at 300°C changes by a factor of about 8. The main cause for the observed effect can be identified to be the variation of the phonon mean free path. The phonon mean free path l is found to be systematically smaller than the microcrystallite size L_a, i.e., the mean free path is controlled by the presence of defects which are partially cured at increasing pyrolysis temperature. Small angle X-ray scattering indicates that structural changes on the length scale between 0.5 and 1 nm are the key for the drastic increase of the thermal conductivity in carbon aerogels with increasing pyrolysis temperature. An investigation of the samples presented here with small angle X-ray scattering is currently in progress.

ACKNOWLEDGMENTS

This work has been supported by the Bavarian Science Foundation in Munich. The authors thank Dr. M. Schreck, University of Augsburg, Germany, for performing the Raman measurements and Dr. D. Kehr, Schunk Kohlenstofftechnik GmbH, Gießen, Germany, for performing the high-temperature treatment of the specimens and valuable discussions.

REFERENCES

1. R. W. Pekala and F. M. Kong, "A Synthetic Route to Organic Aerogels – Mechanism, Structure, and Properties," 2nd *Int. Symp. on Aerogels* (ISA 2), Montpellier, France (1989), C4-33–40.
2. R. Saliger, *Carbon Aerogels for Application in Electrochemical Double Layer Capacitors* (Ph.D. Thesis, University of Würzburg, Germany, Report E21 – 1099 -1, 1999).
3. H. Pröbstle, *Kohlenstoffaerogele für den Einsatz in Superkondensatoren* (Ph.D. Thesis, University of Würzburg, Germany, Report E21 – 1001 – 1, 2001).
4. M. Wiener, *Elektroden aus Kohlenstoffaerogel für PEM-Brennstoffzellen* (Diploma Thesis, University of Würzburg, Germany, Report E21 – 1200 – 1 , 2000).
5. M. Glora, *Charakterisierung von Gasdiffusionsschichten auf der Basis von Kohlenstoff-Aerogelen für PEM-Brennstoffzellen* (Ph.D. Thesis, University of Würzburg, Germany, Report E21 – 0502 – 1, 2002).
6. Y. Hanzawa, H. Hatori, N. Yoshizawa, and Y. Yamada, *Carbon* **40**:575 (2002).
7. L. Soukup, I. Gregora, and L. Jastrabik, *Mater. Sci. Eng.* **B11**:355 (1992).
8. X. Lu, O. Nilsson, J. Fricke, and R. W. Pekala, *J. Appl. Phys*. **73**:583 (1993).
9. O. Nilsson, V. Bock, R. Caps, and J. Fricke, "High Temperature Thermal Properties of Carbon Aerogels," *Thermal Conductivity* 22, *Proc. Twenty-Second Int. Conf. Therm. Conduct.*, T.W. Tong, ed. (1994), pp. 878–887.
10. V. Bock, O. Nilsson, J. Blumm, and J. Fricke, *J. Non-Cryst. Solids* **185**:233 (1995).
11. M. Wiener, G. Reichenauer, T. Scherb, and J. Fricke, *J. Non-Cryst. Solids* **350:**126 (2004).
12. R. L. McCreery, "Carbon Electrodes: Structural Effects on Electron Transfer Kinetics," in *Electroanalytical Chemistry, A Series of Advances*, Vol. 17, A. J. Bard, ed. (Marcel Dekker, New York, 1991), p. 221.
13. D. S. Knight and W. B. White, *J. Mater. Res.* **4**:385 (1989).
14. G. A. M. Reynolds, A. W. P. Fung, Z. H. Wang, M. S. Dresselhaus, and R. W. Pekala, *J. Non-Cryst. Solids* **188**:27 (1995).
15. J. Manara, R. Caps, F. Rather, and J. Fricke, *Optics Commun.* **168**:237 (1999).
16. S. Brunauer, P. H. Emmett, and E. Teller, *J. Am. Ceram. Soc.* **60**:309 (1938).
17. O. Nilsson, H. Mehling, R. Horn, J. Fricke, R. Hofmann, S. G. Müller, R. Eckstein, D. Hofmann, *High Temps. – High Press.* **29**:73 (1997).
18. R. D. Cowan, *J. Appl. Phys*.**34**:926 (1963).
19. National Bureau of Standards, *Special Publication* 260–89 (1984).
20. P. G. Klemens, in *Thermal Conductivity 1*, R. P. Tye, ed. (Academic, London, 1969), p. 1.
21. P. Debye, in *Vorträge über die Kinetische Theorie der Materie und der Elektrizität* (B. G. Teubner, Berlin, 1914), p. 43.
22. G. Reichenauer, A. Emmerling, J. Fricke, and R.W. Pekala, *J. Non-Cryst. Solids* **255**:210 (1998).